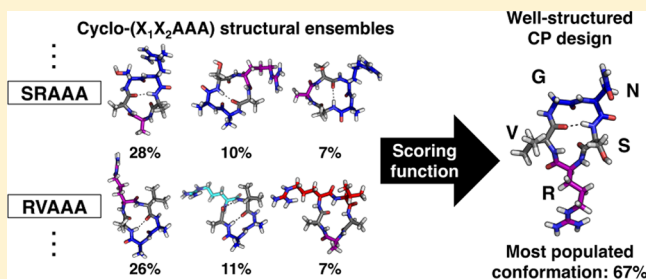


## Designing Well-Structured Cyclic Pentapeptides Based on Sequence–Structure Relationships

Diana P. Slough,<sup>†,§</sup> Sean M. McHugh,<sup>†,§</sup> Ashleigh E. Cummings,<sup>†</sup> Peng Dai,<sup>‡,§</sup> Bradley L. Pentelute,<sup>‡,§</sup> Joshua A. Kritzer,<sup>†,§</sup> and Yu-Shan Lin<sup>†,\*,§</sup><sup>†</sup>Department of Chemistry, Tufts University, Medford, Massachusetts 02155, United States<sup>‡</sup>Department of Chemistry, Massachusetts Institute of Technology, Cambridge, Massachusetts 02139, United States

## S Supporting Information

**ABSTRACT:** Cyclic peptides are a promising class of molecules for unique applications. Unfortunately, cyclic peptide design is severely limited by the difficulty in predicting the conformations they will adopt in solution. In this work, we use explicit-solvent molecular dynamics simulations to design well-structured cyclic peptides by studying their sequence–structure relationships. Critical to our approach is an enhanced sampling method that exploits the essential transitional motions of cyclic peptides to efficiently sample their conformational space. We simulated a range of cyclic pentapeptides from all-glycine to a library of cyclo-(X<sub>1</sub>X<sub>2</sub>AAA) peptides to map their conformational space and determine cooperative effects of neighboring residues. By combining the results from all cyclo-(X<sub>1</sub>X<sub>2</sub>AAA) peptides, we developed a scoring function to predict the structural preferences for X<sub>1</sub>–X<sub>2</sub> residues within cyclic pentapeptides. Using this scoring function, we designed a cyclic pentapeptide, cyclo-(GNSRV), predicted to be well structured in aqueous solution. Subsequent circular dichroism and NMR spectroscopy revealed that this cyclic pentapeptide is indeed well structured in water, with a nuclear Overhauser effect and *J*-coupling values consistent with the predicted structure.



## ■ INTRODUCTION

Cyclic peptides (CPs) have promising applications in nanotechnology,<sup>1–3</sup> as well as potential therapeutics, targeting a variety of protein–protein interactions (PPIs).<sup>4–12</sup> PPIs play critical roles in important and disease-relevant biological processes.<sup>13,14</sup> Modulating PPIs thus provides a means to control diverse cellular functions for both fundamental research and disease intervention.<sup>15,16</sup> Despite the promise of CPs for these applications, de novo design of well-structured CPs in aqueous solution remains challenging. CPs tend to form multiple conformations in solution,<sup>17–28</sup> making them difficult to design or even characterize. Furthermore, the limited availability of solution structural information makes it difficult to develop sequence–structure relationships for CPs. Currently, there is no tractable experimental method to synthesize and characterize the structural ensembles of hundreds of CPs to determine which CPs are well structured, and ultimately to understand how CP sequences control structures.<sup>29–32</sup>

Although experimental determination of structural ensembles is difficult, there have been many promising contributions from computational simulations.<sup>33–51</sup> Recently, we developed a novel, highly efficient enhanced sampling method customized to CPs by identifying their essential transitional motions (coupled two-dihedral angle movements).<sup>49</sup> This enhanced sampling method has made it possible for us to quickly and efficiently sample a CP's structural ensemble, with the inclusion of explicit water.<sup>49–51</sup> This platform produces

more rapidly converged results, allowing us to simulate more systems than was previously possible. This advance has made it much more feasible to gather the broad simulation data needed to study sequence–structure relationships for CPs. In this work, we used this method to systematically simulate over 70 head-to-tail cyclized pentapeptides, uncovered their sequence–structure relationships, and ultimately designed a well-structured CP.

## ■ MATERIALS AND METHODS

**Model Peptides.** The following model peptides were used in this study: cyclo-(GGGGG); cyclo-(X<sub>1</sub>AAAA), where X<sub>1</sub> was any of the 20 standard amino acids; cyclo-(X<sub>1</sub>X<sub>2</sub>AAA), where X<sub>1</sub>/X<sub>2</sub> was G, A, V, F, R, D, N, or S; cyclo-(GFSEV); cyclo-(GNSRV); and cyclo-(GFNDV). Two different initial structures of each CP, S1, and S2 (structure 1 and structure 2, respectively), were prepared using the Chimera molecular modeling package.<sup>52</sup> To construct each CP, the linear peptide was first built, followed by linkage of the N- and C-terminal residues and subsequent energy minimization.

**Bias-Exchange Metadynamics (BE-META) Simulations.** Following preparation in Chimera, each initial structure was solvated using a pre-equilibrated box of water molecules.

Received: February 20, 2018

Revised: March 5, 2018

Published: March 28, 2018



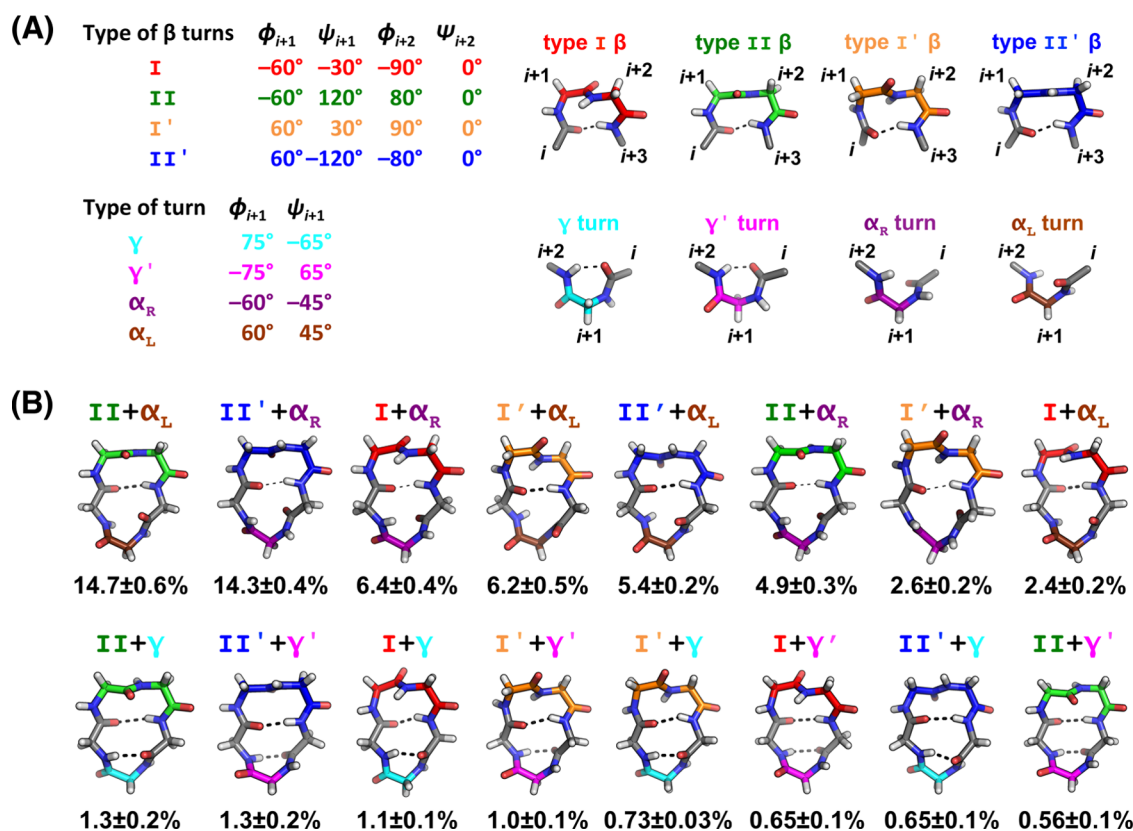


**Figure 1.** Cyclic pentapeptides typically form a  $\beta$  turn plus a tight  $\gamma/\gamma'$  or  $\alpha_R/\alpha_L$  turn opposite the  $\beta$  turn. (A) Ideal dihedral angles, representative structures, and hydrogen bond patterns for the four types of  $\beta$  turns and four types of tight turns. (B) Populations and representative structures for the 16 turn combinations from our BE-META simulations of cyclo-(GGGGG). Types I, I', II, and II'  $\beta$  turns are shown in red, orange, green, and blue, respectively. Tight turns  $\gamma$ ,  $\gamma'$ ,  $\alpha_R$ , and  $\alpha_L$  are shown in cyan, magenta, purple, and brown, respectively. Populations and standard deviation were calculated from the five neutral replicas of the S1 simulations.

Minimal number of ions were added to neutralize the charge of the whole system. Each structure was then energy-minimized using the steepest descent algorithm, followed by a four-step equilibration process. First, to allow the solvent molecules to equilibrate, a 50 ps isochoric–isothermal (NVT) simulation, followed by a 50 ps isobaric–isothermal (NPT) simulation, was performed. In both simulations, a harmonic constraint was placed on the peptide heavy atoms, with a force constant of 1000 kJ/mol nm<sup>2</sup>. Subsequently, a 100 ps NVT simulation, followed by a 100 ps NPT simulation, was performed without any restraints, to equilibrate the entire system. A thermostat of 300 K and a barostat of 1 bar were used for all equilibrations.

The NPT ensemble was used for all BE-META production simulations. The temperature was maintained at 300 K using the V-rescale thermostat,<sup>53</sup> with a time coupling constant of 0.1 ps. The CP and the solvent were coupled to two separate thermostats, to mitigate the “hot solvent–cold solute” problem.<sup>54,55</sup> The pressure was maintained at 1 bar using the Berendsen barostat,<sup>56</sup> with a time coupling constant of 2.0 ps and an isothermal compressibility of  $4.5 \times 10^{-5}$  bar<sup>-1</sup>. All bonds involving hydrogen were constrained using the LINCS algorithm.<sup>57</sup> Dynamics of the system were evolved using the leapfrog algorithm,<sup>58</sup> with a time step of 2 fs. Both short-range Lennard-Jones and electrostatic nonbonded interactions were truncated at 1.0 nm. Beyond the cutoff distance, particle mesh Ewald<sup>59</sup> was used for the electrostatic interactions, with a Fourier spacing of 0.12 nm and an interpolation order of 4. A long-range dispersion correction<sup>60</sup> for the energy and pressure

was used for the Lennard-Jones interaction beyond the cutoff. All trajectories were saved every 1 ps for subsequent analysis.

All simulations were performed using the RSFF2 force field<sup>61</sup> with TIP3P water<sup>62</sup> in Gromacs 4.6.7<sup>63</sup> with the PLUMED 2 plugin.<sup>64</sup> The RSFF2 force field was found to accurately recapitulate several CP crystal structures<sup>48</sup> and therefore will be used throughout this work. Conformational sampling of all CPs was enhanced using BE-META simulations. The collective variables in the BE-META simulations consist of two types of two-dimensional (2D) biases. The first 2D bias is along  $\phi_i \times \psi_i$ , where  $\phi/\psi$  are the backbone dihedral angles of the same residue. The second type of 2D bias is along  $\psi$  of one residue and  $\phi$  of the next residue,  $\psi_i \times \phi_{i+1}$ . These 2D biases were previously found to enhance the conformational sampling of CPs efficiently.<sup>49</sup> Both types of the 2D biases are performed on each residue, giving a total of 10 biased replicas for a cyclic pentapeptide. Gaussian hills were deposited every 4 ps, with a height of 0.1 kJ/mol and a width of 0.314 rad. Exchanges were attempted every 5 ps between different replicas. For analysis of an unbiased structural ensemble, five neutral replicas were added, giving a total of 15 replicas per CP.

**Principal Component and Cluster Analysis.** To characterize the structural ensemble of each CP, the last 50 ns of the unbiased replicas were analyzed using dihedral principal component analysis (dPCA) with the  $\phi$  and  $\psi$  angles of all residues.<sup>65,66</sup> However, if the peptide sequence is homogeneous (i.e., cyclo-(AAAAA)), an additional step needs to be performed prior to dPCA. To take degeneracy into account, the previously developed root-mean-square deviation

(RMSD) scheme was applied.<sup>49</sup> In brief, first the  $\phi/\psi$  dihedral angles of the neutral replicas were calculated. For a cyclic pentapeptide with a homogeneous sequence, there are five ways of reordering each frame. The RMSD to a reference structure was calculated for each of the five permutations, and the structure with the lowest RMSD to the reference structure was used to reorder the CP.

Following dPCA, the population of each cluster was calculated using a density peak-based cluster analysis.<sup>67</sup> For cluster analysis, the principal subspace along the first three principal components (PC1, PC2, and PC3) was divided into  $50 \times 50 \times 50$  grids. Only grids with a population greater than 0.1 were used in cluster analysis. The population of each cluster was determined by summing the population of every grid the cluster contained. dPCA and cluster analysis was used to analyze the structural ensembles of cyclo-(X<sub>1</sub>AAAA), cyclo-(X<sub>1</sub>X<sub>2</sub>AAA), cyclo-(GFSEV), cyclo-(GNSRV), and cyclo-(GFDNV).

Simulation convergence was monitored using the normalized integrated product<sup>38</sup> of the density profiles along PC1, PC2, and PC3 of the S1 and S2 simulations. Convergence was achieved when the density profiles were similar. Final simulation lengths ranged from 100 to 300 ns. All further analysis was performed on the S1 simulations.

**Cutoff Turn Analysis.** Because of their highly constrained nature, cyclic pentapeptides typically form structures containing a  $\beta$  turn plus a tight turn on the opposite side of the CP. The four commonly observed  $\beta$  turns and tight turns give a total of 16 turn combinations (Figure 1A). However, for cyclo-(GGGGG), dPCA and cluster analysis did not identify all 16 turn combinations. To determine whether all turn combinations were present in cyclo-(GGGGG), turns were identified if the  $\phi/\psi$  dihedral angles were within 35° of the ideal values for a specific type of turn (Figure 1A). Similarly, this cutoff-based turn type analysis was used to compare all 16 types of turn combinations in the cyclo-(X<sub>1</sub>AAAA) and cyclo-(X<sub>1</sub>X<sub>2</sub>AAA) pentapeptides (Figures 3A and S1), as the dPCA–cluster analysis was unable to pick up combinations with very low populations.

**Logo Plot for Individual Amino Acids from Cyclo-(X<sub>1</sub>AAAA) Simulations.** To determine the most probable amino acid for each position of a given turn combination, we weighted X<sub>1</sub> in cyclo-(X<sub>1</sub>AAAA) using the following scheme. The preference of the amino acid X<sub>1</sub>, when X<sub>1</sub> ≠ A, for each of the five locations within a given turn combination was determined by its population from the cutoff turn analysis. In the case of cyclo-(AAAAA), there are five degenerate amino acids, and the population was divided by five for the associated position in the logo plot. The logo plot for cyclo-(X<sub>1</sub>AAAA) for the  $\beta_{II'} + \alpha_R$  turn combination is shown in Figure 4A.

**Neighbor Analysis for X<sub>1</sub>X<sub>2</sub> from Cyclo-(X<sub>1</sub>X<sub>2</sub>AAA) Simulations.** To help design well-structured cyclic peptides, a scoring function based on neighboring residues was developed using the simulation results of cyclo-(X<sub>1</sub>X<sub>2</sub>AAA), where X<sub>1</sub>/X<sub>2</sub> is G, V, F, R, D, N, and S. To evaluate the preference score for a sequence cyclo-(X<sub>1</sub>X<sub>2</sub>X<sub>3</sub>X<sub>4</sub>X<sub>5</sub>) to adopt a specific  $\beta$  turn at X<sub>1</sub>X<sub>2</sub> and a specific tight turn at X<sub>4</sub>, the sequence was broken down into five sets of nearest neighbor pairs, X<sub>1</sub>X<sub>2</sub>, X<sub>2</sub>X<sub>3</sub>, X<sub>3</sub>X<sub>4</sub>, X<sub>4</sub>X<sub>5</sub>, and X<sub>5</sub>X<sub>1</sub>, and the total preference score was the sum of the five populations for each pair to adopt the desired structure in the simulations of cyclo-(X<sub>1</sub>X<sub>2</sub>AAA), cyclo-(X<sub>2</sub>X<sub>3</sub>AAA), etc. For example, the score for sequence cyclo-(X<sub>1</sub>X<sub>2</sub>X<sub>3</sub>X<sub>4</sub>X<sub>5</sub>) adopting a type II'  $\beta$  turn at X<sub>1</sub>X<sub>2</sub> and an  $\alpha_R$  turn at X<sub>4</sub> was calculated as

follows. We analyzed the structural ensemble of cyclo-(X<sub>1</sub>X<sub>2</sub>AAA) using the cutoff-based turn analysis to evaluate the population of cyclo-(X<sub>1</sub>X<sub>2</sub>AAA) that adopts a type II'  $\beta$  turn at X<sub>1</sub>X<sub>2</sub> and an  $\alpha_R$  turn at X<sub>4</sub>, the population of cyclo-(AX<sub>2</sub>X<sub>3</sub>AA) that adopts a type II'  $\beta$  turn at <sup>1</sup>AX<sup>2</sup> and an  $\alpha_R$  turn at X<sub>4</sub>, the population of cyclo-(AA<sub>2</sub>X<sub>3</sub>AA) that adopts a type II'  $\beta$  turn at <sup>1</sup>AA<sup>2</sup> and an  $\alpha_R$  turn at X<sub>4</sub>, etc. The score was then calculated as the sum of these five populations, when each pair is located at the desired location of the target turn combination (example for cyclo-(GNSRV) shown in Figure 5A).

**Thermodynamics Decomposition.** To further understand the structural ensemble of a CP, we performed thermodynamics decomposition of the S1 simulation.  $\Delta G$  between clusters was calculated using the Boltzmann equation, using the ratios of cluster populations and the most populated cluster as a reference.  $\Delta G$  was then further separated into  $\Delta H$  and  $\Delta S$ , where  $\Delta H$  was estimated from the difference in potential energy between clusters.  $\Delta H$  was then further decomposed into peptide in vacuum ( $\Delta H_p^{\text{vac}}$ ) and the rest ( $\Delta H_{\text{rest}}$ ). To perform this decomposition, the potential energy of two groups was calculated: peptide and solvent/ions (note that ions may not be present in all systems). The peptide enthalpy ( $\Delta H_p^{\text{vac}}$ ) consisted of peptide Lennard-Jones ( $\Delta H_p^{\text{LJ}}$ ), short-range and 1,4 electrostatics ( $\Delta H_p^{\text{EE}(\text{SR}+1,4)}$ ), bonds ( $\Delta H_p^{\text{bond}}$ ), angles ( $\Delta H_p^{\text{angle}}$ ), proper dihedrals ( $\Delta H_p^{\text{dih}}$ ), and improper dihedrals ( $\Delta H_p^{\text{imp}}$ ).  $\Delta S$  was further decomposed into configurational entropy of the peptide ( $\Delta S_p^{\text{conf}}$ ) and solvation entropy ( $\Delta S_w$ ).  $\Delta S_p^{\text{conf}}$  was calculated using the maximum information spanning tree<sup>68–70</sup> method, and  $\Delta S_w$  was calculated using  $\Delta S_w = \Delta S - \Delta S_p^{\text{conf}}$ .

**Linear Peptide Synthesis.** The linear peptides were synthesized at 0.04 mmol scale on HMPB-ChemMatrix resin (PCAS BioMatrix Inc., loading = 0.5 mmol/g). The linear peptides were prepared with C-terminal glycine to facilitate head-to-tail cyclization. The HMPB resin was firstly functionalized with glycine: 5 mmol Fmoc-glycine-OH and 2.5 mmol N,N'-diisopropylcarbodiimide were dissolved in 15 mL dimethylformamide (DMF). After 10 min at room temperature, the mixture was added to 0.75 g of HMPB resin in a 20 mL Torviq fritted syringe. After another 1 min, 0.05 mmol 4-dimethylaminopyridine was added and reacted at room temperature for 16 h, followed by three times wash with DMF, twice 5 min deprotection with 20% (v/v) piperidine in DMF, and four times wash with DMF. The resin was washed thoroughly with dichloromethane (DCM) and dried under vacuum. The following solid-phase peptide synthesis (SPPS) was carried out on a synthesizer for automated flow peptide synthesis.<sup>71</sup> After completion of the SPPS, the resin was washed thoroughly with DCM and dried under vacuum. The resins were transferred to a 50 mL plastic tube and the peptide was simultaneously cleaved from the resin and side-chain deprotected by treatment with 2.5% (v/v) water, 2.5% (v/v) 1,2-ethanedithiol, and 1% (v/v) triisopropylsilane in neat trifluoroacetic acid (TFA) for 2 h at room temperature. The resulting solution containing peptide was triturated and washed with cold diethyl ether (prechilled in –80 °C freezer) two times. The obtained gummylike solid was dissolved in 50% H<sub>2</sub>O/50% acetonitrile containing 0.1% TFA and lyophilized.

**Peptide Cyclization and Purification.** The lyophilized crude peptide was directly used for cyclization. Cyclization condition: 0.5 mM peptide, 1.5 mM 1-[bis(dimethylamino)-methylene]-1H-1,2,3-triazolo[4,5-b]pyridinium 3-oxid hexafluorophosphate, 3 mM N,N-diisopropylethylamine, DMF as



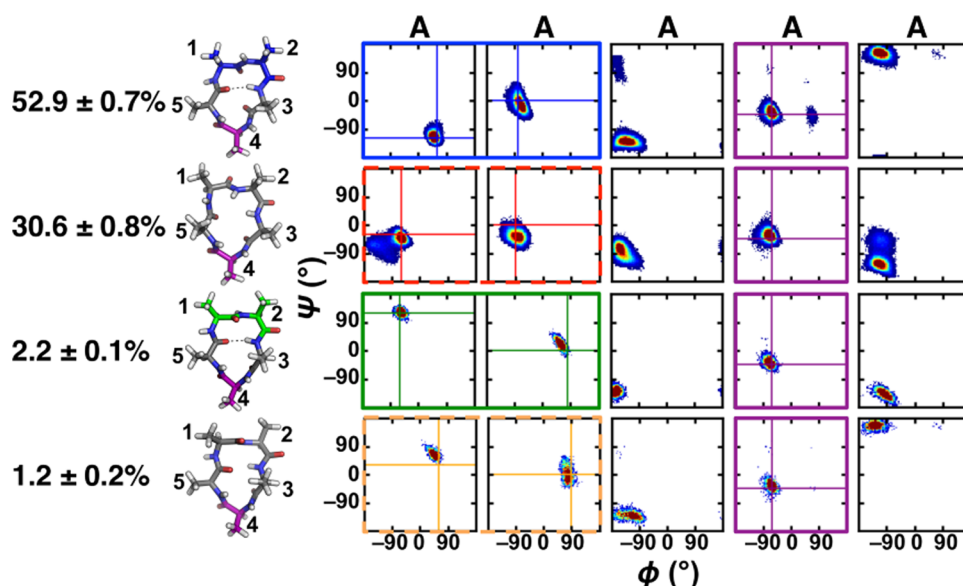


**Figure 2.** Populations, representative structures, and Ramachandran plots for the top four clusters of cyclo-(AAAAA). Type II  $\beta$ , type II'  $\beta$ , and  $\alpha_R$  turns are shown and boxed in the Ramachandran plots in green, blue, and purple, respectively. Distorted type I and I'  $\beta$  turns are boxed in the Ramachandran plots by red and orange dashed lines, respectively. Populations and standard deviations were calculated from the five neutral replicas of the S1 simulation.

solvent, room temperature for 1 h. The cyclization reaction was quenched by adding TFA. After removing solvents by rotary evaporator, the reaction mixture was redissolved in water containing 10% dimethyl sulfoxide and purified on Agilent 1260 Infinity Automated LC/MS Purification System, with a semipreparative reverse phase-high-performance liquid chromatography (HPLC) column (Agilent Zorbax 300SB C<sub>3</sub> column: 21.2  $\times$  250 mm<sup>2</sup>, 7  $\mu$ m, linear gradient: 1–41% B over 80 min, flow rate: 4 mL/min). The purity of fractions was confirmed by liquid chromatography mass spectrometry (LC–MS) analysis. The fractions containing pure cyclized peptide were combined and lyophilized to yield cyclized peptide powder.

**NMR Characterization.** The peptide was dissolved in H<sub>2</sub>O/D<sub>2</sub>O (90:10) at a concentration of roughly 3.5 mM. One-dimensional (1D) and 2D <sup>1</sup>H NMR spectra were recorded on a Bruker 600 MHz spectrometer with CryoProbe at 288 K. Complete resonance assignments were made using homo-nuclear <sup>1</sup>H–<sup>1</sup>H total correlation spectroscopy (TOCSY) and rotating-frame Overhauser spectroscopy (ROESY) experiments. Standard pulse programs available from the Bruker library were used, with mixing times of 60 ms for the TOCSY and 250 ms for the ROESY. <sup>1</sup>H chemical shifts were referenced to 4,4-dimethyl-4-silapentane-1-sulfonic acid ( $\delta$  0.00 ppm) in water. <sup>3</sup>J<sub>NH</sub> C<sub>H $\alpha$</sub>  coupling constants were measured from 1D <sup>1</sup>H NMR.

**Circular Dichroism (CD) Characterization.** Compounds were dissolved in water to concentrations of 87.5  $\mu$ M, as measured by peptide weight. Equal concentrations of the peptides were verified prior to CD analysis by subjecting peptides to analytical HPLC and normalizing on the basis of peak volumes. CD spectra were obtained on a Jasco J-815 CD Spectrometer at 20  $^{\circ}$ C using the following measurement parameters: wavelength range, 190–260 nm; step resolution, 0.5 nm; speed, 20 nm/min; accumulations, 3; response, 1 s; bandwidth, 1 nm; and path length, 0.1 cm.

## RESULTS AND DISCUSSION

### Structural Ensembles of Cyclo-(GGGGG) and Cyclo-(X<sub>1</sub>AAAA) Map Out the Available Conformational Space for Simple Cyclic Pentapeptides.

Cyclic pentapeptides typically form a  $\beta$  turn plus a tight turn opposite the  $\beta$  turn.<sup>72–79</sup> There are four types of  $\beta$  turns ( $\beta_I$ ,  $\beta_{II}$ ,  $\beta_{I'}$ , and  $\beta_{II'}$ ) and four types of tight turns ( $\gamma$ ,  $\gamma'$ ,  $\alpha_R$ , and  $\alpha_L$ ) that are commonly observed (Figure 1A), leading to 16 possible turn combinations for cyclic pentapeptides. A cyclic pentapeptide with a  $\beta$  turn and a tight turn of  $\gamma$  or inverse- $\gamma$  ( $\gamma'$ ) tends to form two intrapeptide hydrogen bonds (Figure 1B, bottom row), whereas a cyclic pentapeptide having a  $\beta$  turn and a tight turn with a dihedral angle of a right-handed or left-handed  $\alpha$ -helix ( $\alpha_R$  and  $\alpha_L$ , respectively) will form only one intrapeptide hydrogen bond (at the  $\beta$  turn site; Figure 1B, top row). All of these 16 turn combinations were seen in our bias-exchange metadynamics (BE-META) simulations of cyclo-(GGGGG) and are shown in Figure 1B. The most populated conformation was a  $\beta_{II} + \alpha_L$  with a population of  $14.7 \pm 0.6\%$ . We observed that the mirror-image turn combination,  $\beta_{II'} + \alpha_R$ , has a population ( $14.3 \pm 0.4\%$ ) similar to that of  $\beta_{II} + \alpha_L$ . Because glycine is achiral, theoretically, conformations that are mirror images of each other should have exactly the same population. In our simulations of cyclo-(GGGGG), each conformation and its mirror image indeed had similar populations (Figure 1B), further supporting convergence of our simulation results.

Among the 16 turn combinations observed in cyclo-(GGGGG), all clusters with an  $\alpha_R/\alpha_L$  turn (top row of Figure 1B) were more populated than clusters with a  $\gamma/\gamma'$  turn (bottom row of Figure 1B). To further understand this structural preference of cyclo-(GGGGG), we performed thermodynamics decomposition on the 16 clusters (Table S1). The thermodynamics of clusters 1 and 2 were almost identical, which is consistent with the fact that they are mirror images of each other ( $\beta_{II} + \alpha_L$  vs  $\beta_{II'} + \alpha_R$ ). The third and fourth most populated clusters,  $\beta_I + \alpha_R$  and  $\beta_{I'} + \alpha_L$ , had more favorable solvation enthalpy compared to the most populated

clusters. However, they both had an unfavorable peptide enthalpy relative to the top clusters (most populated clusters;  $\beta_{II} + \alpha_L$  and  $\beta_{II'} + \alpha_R$ ), arising from unfavorable electrostatics, angles, and dihedrals. Clusters 5 and 6 formed the  $\beta_{II'} + \alpha_L$  and  $\beta_{II} + \alpha_R$  turn combinations, respectively, and were less stable than the most populated clusters due to peptide electrostatics and dihedrals. The least populated turn combinations involving  $\alpha_L$  and  $\alpha_R$ ,  $\beta_I + \alpha_R$  and  $\beta_I + \alpha_L$  (clusters 7 and 8) had unfavorable peptide angles and dihedrals compared with the most populated cluster.

In contrast to clusters 1–8, clusters 9–16 formed a  $\gamma/\gamma'$  turn instead of adopting an  $\alpha_R/\alpha_L$  conformation. Because clusters with a  $\gamma/\gamma'$  turn form two intrapeptide hydrogen bonds, their peptide electrostatics were more favorable than those of the most populated cluster (Table S1). However, clusters with a  $\gamma/\gamma'$  turn all had unfavorable angles and dihedrals as well as unfavorable solvation enthalpy, relative to the top cluster. A combination of these factors makes clusters with  $\gamma/\gamma'$  turns have lower populations than their  $\alpha_R/\alpha_L$  counterparts.

Moving from achiral glycine to the simplest all L-amino acid peptide, cyclo-(AAAAA), we expected turn combinations involving an  $\alpha_R$  turn to be preferred over an  $\alpha_L$  turn, on the basis of the  $\phi$  angle preferences for an L-amino acid. The four most populated clusters of cyclo-(AAAAA) from our BE-META simulation are shown in Figure 2, and indeed all of these turn combinations had a tight  $\alpha_R$  turn rather than a tight  $\alpha_L$  turn, corresponding to clusters 2, 3, 6, and 7, respectively, in Figure 1B for cyclo-(GGGGG). Similar to cyclo-(GGGGG),  $\beta_{II'} + \alpha_R$  was the most favorable turn combination, with a population of  $52.9 \pm 0.7\%$ . The second most populated cluster formed a distorted type  $\beta_I + \alpha_R$ , where the distorted type I  $\beta$  turn had nearly ideal dihedral angles for a type I  $\beta$  turn, but deviation in the  $\psi$  angle of the  $i + 2$  residue results in a turn that does not frequently form a hydrogen bond.

Breaking down the thermodynamics of cyclo-(AAAAA), the distorted  $\beta_I + \alpha_R$  cluster had less favorable electrostatics and dihedrals compared with the most populated  $\beta_{II'} + \alpha_R$  turn combination (Table S2). The third and fourth most populated clusters formed a  $\beta_{II} + \alpha_R$  and a distorted type  $\beta_I + \alpha_R$ , and compared with cyclo-(GGGGG), the preferred order of all of the  $\alpha_R$ -containing clusters remained the same. Both clusters 3 and 4 were less favorable than the most populated cluster due to entropy, specifically peptide configurational entropy. Looking at the peptide contribution to the thermodynamics, clusters 3 and 4 have poor electrostatics and cluster 4 (distorted  $\beta_I + \alpha_R$ ) also had unfavorable angles compared with the most populated  $\beta_{II'} + \alpha_R$  (Table S2).

Overall, for the thermodynamics of cyclo-(GGGGG), we found that the most populated conformation and its mirror-image counterpart are stabilized over the other clusters via either peptide or solvation enthalpy. The most populated conformation of cyclo-(AAAAA), on the other hand, is entropically more favorable than the other clusters due to either configurational or solvation entropy. The complex balance between peptide enthalpy, solvation enthalpy, and entropy for these two simple cyclic pentapeptide systems reaffirms the necessity of using explicit water in CP simulations to accurately describe each thermodynamic factor.

**Structural Ensembles of Cyclo-(X<sub>1</sub>AAAA) Show Structural Preferences of Each Amino Acid.** To understand how different amino acids affect structural preferences of a cyclic pentapeptide, we performed BE-META simulations of cyclo-(X<sub>1</sub>AAAA), where X<sub>1</sub> was any of the 20 basic amino acids. The

population and turn combination of the three most populated clusters for each of these 20 sequences are given in Table S3. We found that the turn combination  $\beta_{II'} + \alpha_R$  was by far the most prevalent, accounting for  $\sim 75\%$  of all of the turn combinations that form for these 20 CPs (Figure 3A). The second most populated turn combination was a distorted  $\beta_I + \alpha_R$  ( $\sim 14\%$ ). Although  $\beta_{II'} + \alpha_R$  predominated among the turn combinations observed for these 20 CPs, the locations of the type II'  $\beta$  turn and the  $\alpha_R$  residue varied within the X<sub>1</sub>AAAA sequence (Figure 3B and Table S3).

By combining the results from all 20 cyclo-(X<sub>1</sub>AAAA) CPs, we constructed a logo plot showing the probability of each amino acid for each location in the  $\beta_{II'} + \alpha_R$  turn combination (Figure 4A). We hypothesized that combining the most probable amino acid at every position of the  $\beta_{II'} + \alpha_R$ -structured cyclic pentapeptide would produce a sequence that adopts a well-structured conformation. On the basis of the results shown in Figure 4A, the sequence, cyclo-(GFSEV), was predicted to be the most structured for a  $\beta_{II'} + \alpha_R$  turn combination, with the  $\beta_{II'}$  turn located at <sup>1</sup>GF<sup>2</sup> and  $\alpha_R$  turn located at E<sup>4</sup>. To verify this prediction, this designed sequence was simulated using BE-META simulations to characterize its structural ensemble. The most populated cluster ( $54.8 \pm 0.6\%$ ) of cyclo-(GFSEV) was indeed the  $\beta_{II'} + \alpha_R$  turn combination, with the type II'  $\beta$  turn at <sup>1</sup>GF<sup>2</sup> and a tight  $\alpha_R$  turn at E<sup>4</sup> (Figure 4B). However, this population ( $\sim 55\%$ ) was not significantly higher than the most populated cluster of simple cyclo-(AAAAA) ( $\sim 53\%$ ). This result suggests that the structural preferences for each of the 20 amino acids within cyclo-(X<sub>1</sub>AAAA) are not necessarily additive, implying that neighboring residues might affect each other's structural preferences. This would explain why merely using results from cyclo-(X<sub>1</sub>AAAA) studies did not enable design of a particularly well-structured cyclic pentapeptide.

**Structural Ensembles of Cyclo-(X<sub>1</sub>X<sub>2</sub>AAA) Reveal Cooperative Effects between Neighboring Amino Acids.** To understand the effects of neighboring amino acids on the structural ensemble of a cyclic pentapeptide, we performed BE-META simulations of cyclo-(X<sub>1</sub>X<sub>2</sub>AAA), where X<sub>1</sub>/X<sub>2</sub> was G, A, V, F, R, D, N, or S. These eight amino acids were chosen as a representative subsection of the 20 basic amino acids. The populations and turn combinations of the three most populated clusters for each of these 56 sequences is given in Table S4. Similar to cyclo-(X<sub>1</sub>AAAA), most of the top clusters formed a tight  $\alpha_R$  turn, which is consistent with the  $\phi$  angle preferences for an L-amino acid. However, there were a few instances where a  $\gamma$  turn occurs in the top three clusters. Nonetheless, we observed that  $\beta_{II'} + \alpha_R$  remains the most prevalent in all 56 cyclo-(X<sub>1</sub>X<sub>2</sub>AAA) CPs, similar to cyclo-(X<sub>1</sub>AAAA) (Figure S1 compared to Figure 3A). In fact,  $\beta_{II'} + \alpha_R$  was the most populated cluster for 49 out of the 56 sequences. However, turn locations varied in the top clusters forming  $\beta_{II'} + \alpha_R$ , depending on their sequences.

**Rational Design of Well-Structured CPs.** To help design a well-structured cyclic pentapeptide, we used the structural ensemble results of cyclo-(X<sub>1</sub>X<sub>2</sub>AAA) CPs to develop a scoring function based on the observed populations for the desired conformation. The scoring function combined the structural preferences of each neighboring pair (X<sub>1</sub>X<sub>2</sub>, X<sub>2</sub>X<sub>3</sub>, etc.) in a cyclic pentapeptide cyclo-(X<sub>1</sub>X<sub>2</sub>X<sub>3</sub>X<sub>4</sub>X<sub>5</sub>) for a specific conformation (see "Neighbor Analysis for X<sub>1</sub>X<sub>2</sub> from Cyclo-(X<sub>1</sub>X<sub>2</sub>AAA) Simulations" in Materials and Methods). Because alanine was a common filler amino acid in the cyclo-

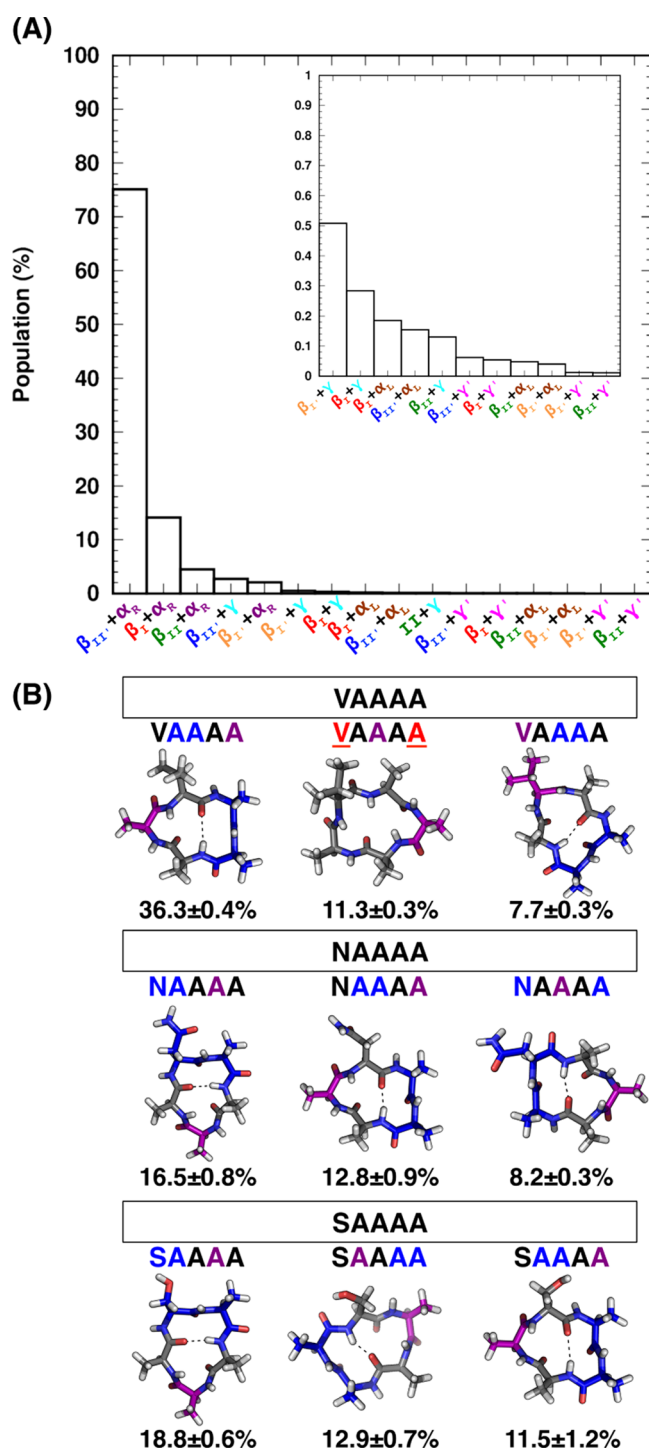


**Figure 3.** (A) Populations of 16 turn combinations from simulations of cyclo-( $X_1$ AAAA). Results use the cutoff turn analysis (see [Materials and Methods](#) for analysis details). (B) Populations and representative structures of the three most populated clusters of cyclo-(VAAAA), cyclo-(NAAAA), and cyclo-(SAAAA). Type II'  $\beta$  turn and  $\alpha_R$  turn are shown and their locations in the sequences highlighted in blue and purple, respectively. The location of distorted type I  $\beta$  turn in the sequence is highlighted in red and underlined. Populations and standard deviations were calculated from the five neutral replicas of the S1 simulations.

( $X_1X_2$ AAA) data set, we ignored A and only analyzed structural preferences and developed scoring functions for  $X_1X_2$  pairs, where  $X_1/X_2$  was G, V, F, R, D, N, or S. The sequences and

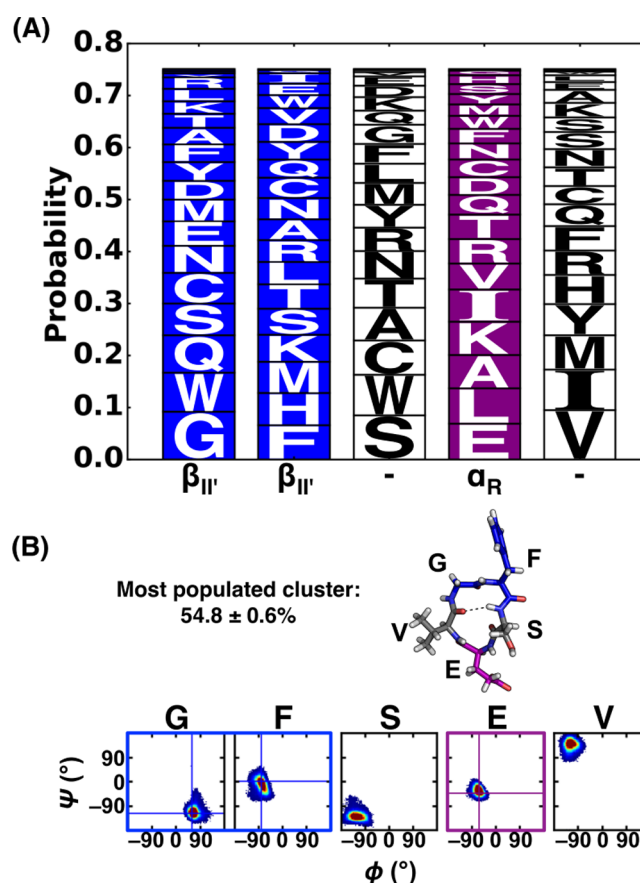


**Figure 4.** (A) Logo plot for cyclo-( $X_1$ AAAA) with the  $\beta_{II'} + \alpha_R$  turn combination. Results use cutoff turn analysis of the S1 simulations (see [Materials and Methods](#) for analysis details). Type II'  $\beta$  turn and  $\alpha_R$  turn are shown, and their locations in the sequences highlighted in blue and purple, respectively. (B) Population, representative structure, and Ramachandran plot for the most populated cluster of cyclo-(GFSEV). Type II'  $\beta$  turn and  $\alpha_R$  turn are shown in blue and purple boxes, respectively. The population and standard deviation was calculated from the five neutral replicas of the S1 simulation.

scores for the 20 highest-scoring cyclo-( $X_1X_2X_3X_4X_5$ ) sequences for the  $\beta_{II'} + \alpha_R$  turn combination, with a type II'  $\beta$  turn at  $X_1X_2$  and an  $\alpha_R$  turn at  $X_4$ , are given in [Table S5](#). Of all 16 807 sequences, cyclo-(GNSRV) received the highest score (1.287) for the  $\beta_{II'} + \alpha_R$  turn combination ([Figure 5A](#) and highlighted in blue in [Figure 5B](#)). To verify this prediction, BE-META simulations of cyclo-(GNSRV) were performed. The simulation results revealed a well-structured conformational ensemble, with the most populated cluster forming a type II'  $\beta$  turn at  $^1\text{GN}^2$  and a tight  $\alpha_R$  turn at  $\text{R}^4$ , as predicted by the scoring function, with a population of 67% ([Figure 6A](#)).

To further understand why cyclo-(GNSRV) is well-structured, we performed thermodynamics decomposition on this peptide and on the five parent cyclo-( $X_1X_2$ AAA) peptides that contain the five relevant neighbor pairs ([Table S6](#)). Comparing the location of the turns in cyclo-(GNSRV) to the locations of the turns in the five parent sequences, cyclo-(GNAAG), cyclo-(AAARV), and cyclo-(GAAAV) all had the  $\beta_{II'} + \alpha_R$  turns at the same location as cyclo-(GNSRV) in the most populated cluster. However, in cyclo-(ANSAA) and cyclo-(AASRA), the  $\beta_{II'} + \alpha_R$  turn combination corresponding to cyclo-(GNSRV) occurred as the third and second most populated clusters, respectively. The comparison of the



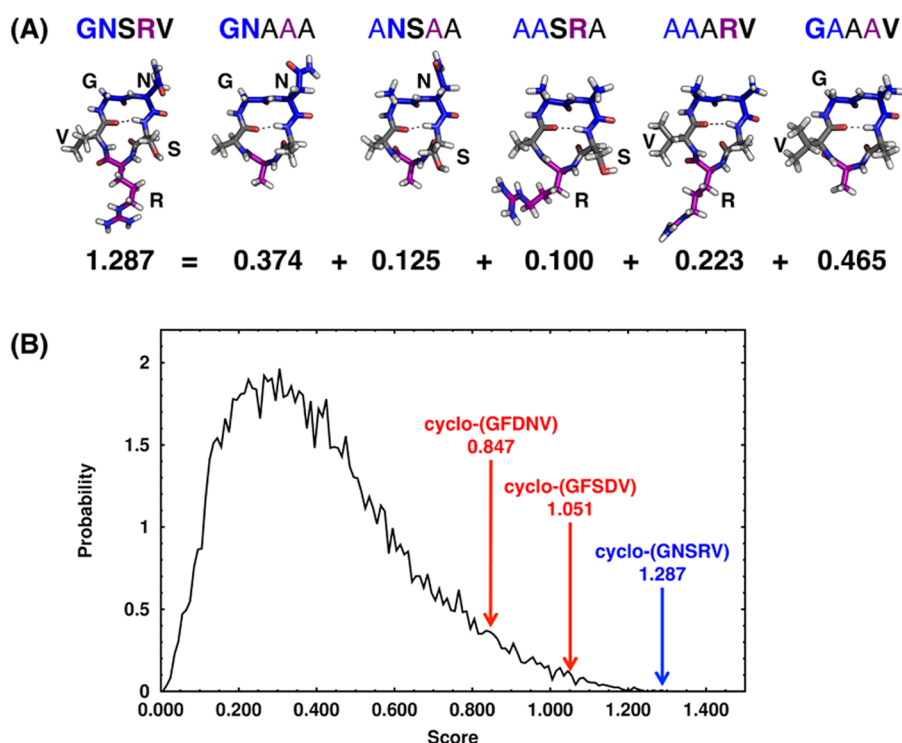


**Figure 5.** Cyclo-(GNSRV) was predicted to have high preference to adopt a  $\beta_{II'}$  +  $\alpha_R$  turn combination on the basis of neighbor-pair scoring. (A) (Top)  $\beta_{II'}$  +  $\alpha_R$  turn combination for cyclo-(GNSRV) and its five parent sequences: cyclo-(GNAAA), cyclo-(ANSAA), cyclo-(AASRA), cyclo-(AAARV), and cyclo-(GAAAV). Neighbor pairs are bolded, and type II'  $\beta$  turn and tight turn  $\alpha_R$  are shown in blue and purple, respectively. (Bottom) Neighbor scores, which were calculated using cutoff analysis for the corresponding  $\beta_{II'}$  +  $\alpha_R$  turn combination. (B) Distribution of scores for the  $\beta_{II'}$  +  $\alpha_R$  turn combination for the 16 807 sequences of cyclo-( $X_1X_2X_3X_4X_5$ ), where  $X_1/X_2/X_3/X_4/X_5$  were G, V, F, R, D, N, or S. Well-structured CP cyclo-(GNSRV) and its score is highlighted in blue. Cyclo-(GFSDV), the proxy of cyclo-(GFSEV), from simulations of cyclo-( $X_1$ AAAA) and cyclo-(GFDNV) and their associated scores are highlighted in red.

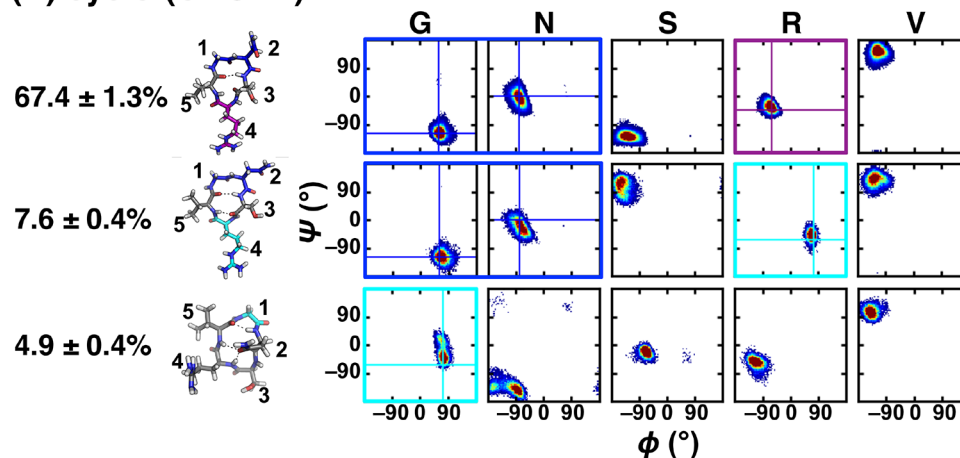
thermodynamics of cyclo-(GNSRV) and the five parent sequences shows that a variety of factors stabilized the most populated clusters and that these factors are generally consistent among the five neighbor-pair peptides and cyclo-(GNSRV). For example, the most populated cluster of cyclo-(GNSRV), cyclo-(AAARV), and cyclo-(GAAAV) formed a  $\beta_{II'}$  +  $\alpha_R$ , whereas the second most populated cluster formed a  $\beta_{II'}$  +  $\gamma$  with the  $\gamma$  turn at the same residues as the  $\alpha_R$  turn. In all three simulations, the top clusters were stabilized over the second clusters due to enthalpy. Specifically, even though the  $\beta_{II'}$  +  $\gamma$  clusters have more favorable intrapeptide electrostatics, they have more unfavorable dihedrals and much more unfavorable solvation enthalpy as compared to those of the most populated cluster. Interestingly, the most populated conformation of cyclo-(GNSRV) is both enthalpically and entropically stabilized over clusters 2 and 3. This is unlike any of the five parent sequences, whose most populated cluster is stabilized by either enthalpy or entropy alone.

Previously, using the simulation results of cyclo-( $X_1$ AAAA), where  $X_1$  was any of the 20 basic amino acids, cyclo-(GFSEV) was predicted to have the highest preference for the  $\beta_{II'}$  +  $\alpha_R$  turn combination. However, BE-META simulations of cyclo-(GFSEV) showed that the population of the desired structure ( $\beta_{II'}$  +  $\alpha_R$ ) was only 55%, a modest improvement from the 53% in cyclo-(AAAAA). Indeed, when using the scoring functions derived from the cyclo-( $X_1X_2$ AAA) simulations results, the score for the  $\beta_{II'}$  +  $\alpha_R$  conformation for cyclo-(GFSDV), the proxy of cyclo-(GFSEV) because in the cyclo-( $X_1X_2$ AAA) data set,  $X_1/X_2$  could only be G, V, F, R, D, N, or S, ranked poorly at number 277, with a score of 1.051 (highlighted in red in Figure

5B). This observation verified the importance of incorporating the neighboring effects in scoring the cyclic peptide's structural preference.

**Predicted  $\beta_{II'}$  +  $\alpha_R$  Structure of Cyclo-(GNSRV) Is Supported by NMR.** To corroborate our simulation predictions, we synthesized cyclo-(GNSRV) and characterized its structure in aqueous solution. NMR spectroscopy provided high-resolution data describing the structural ensemble of cyclo-(GNSRV) in water. The 1D spectrum and 2D spectra from ROESY and TOCSY experiments provided ample evidence that cyclo-(GNSRV) was well structured in water (Figures S2–S5), and these data were wholly consistent with the predicted type II'  $\beta$  turn at  $^1\text{GN}^2$  and  $\alpha_R$  turn at  $\text{R}^4$  (Tables S7 and S8). Overall, protons had unique, well-resolved and well-dispersed chemical shifts, consistent with a single predominant structure. We observed several nuclear Overhauser effects (NOEs) that support the predicted  $\beta_{II'}$  +  $\alpha_R$  structure. For example, for types I and I'  $\beta$  turns, the distance between the  $\text{H}_\text{N}$  protons of the  $i + 1$  and  $i + 2$  residues and the distance between the  $\text{H}_\text{N}$  protons of the  $i + 2$  and  $i + 3$  residues are both small ( $<3$  Å); on the other hand, in types II and II'  $\beta$  turns, only the distance between the  $\text{H}_\text{N}$  protons of the  $i + 2$  and  $i + 3$  residues is small ( $<3$  Å) (Figure 1A). In the ROESY spectra of cyclo-(GNSRV), we observed a strong NOE between  $\text{Asn}^2(\text{H}_\text{N})$  and  $\text{Ser}^3(\text{H}_\text{N})$  but no NOE was observed between  $\text{Gly}^1(\text{H}_\text{N})$  and  $\text{Asn}^2(\text{H}_\text{N})$  (Figures 7A, S6, and Table S7). The presence of this specific  $\text{H}_\text{N}$ – $\text{H}_\text{N}$  NOE and the lack of the other NOE provides strong support for a type II or II'  $\beta$  turn at residues  $^1\text{GN}^2$ , rather than a type I or I'  $\beta$  turn. Similarly, the distance between the  $\text{H}_\text{N}$  protons of the  $i + 1$  and  $i + 2$  residues

## (A) cyclo-(GNSRV)



## (B) cyclo-(GFDNV)

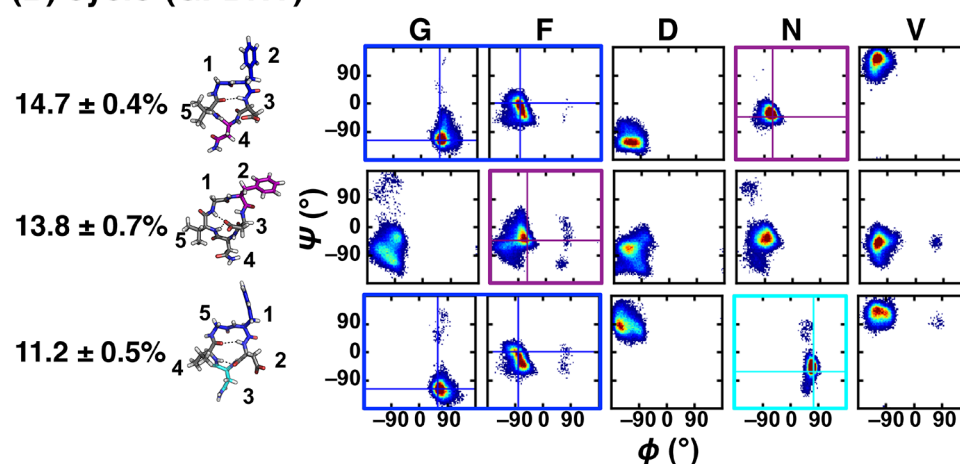


**Figure 6.** Populations, representative structures, and Ramachandran plots for the top three clusters of (A) cyclo-(GNSRV) and (B) cyclo-(GFDNV). Type II'  $\beta$  turns are shown in blue boxes. Tight turns  $\gamma$  and  $\alpha_R$  are shown in cyan and purple boxes, respectively. Populations and standard deviations were calculated from the five neutral replicas of the S1 simulation.

is only small in a  $\alpha_R$  or  $\alpha_L$  turn but not in a  $\gamma$  or  $\gamma'$  turn (Figure 1A). We observed a strong NOE between Arg<sup>4</sup>(H<sub>N</sub>) and Val<sup>5</sup>(H<sub>N</sub>) (Figure S6 and Table S7), which supports an  $\alpha_R$  turn centered at Arg<sup>4</sup>.  $J$  values allowed estimation of the  $\phi$  angle for Arg<sup>4</sup> at  $-60 \pm 30^\circ$  (Figure S6 and Table S8), which is consistent with an  $\alpha_R$  turn rather than an  $\alpha_L$  turn. Similarly, the  $\phi$  angles for Ser<sup>3</sup> and Val<sup>5</sup> were estimated at  $-120 \pm 30^\circ$  on the basis of the  $J$  values, which are also in agreement with the predicted structure (Figures 6A, S6, and Table S8).

#### Design of an Unstructured Control for Cyclo-(GNSRV).

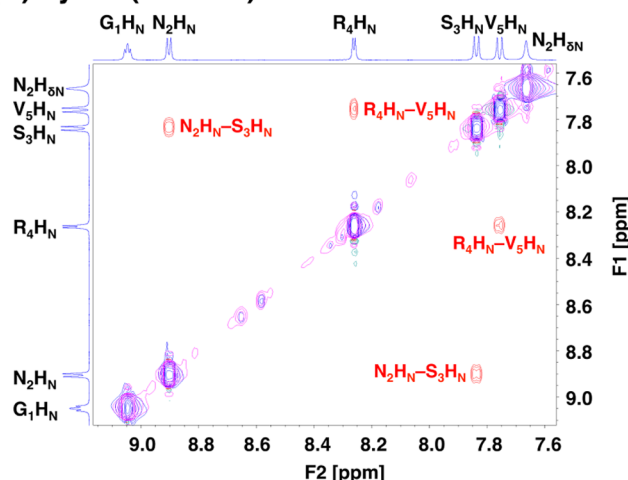
We observed that one of the parent sequences of the well-structured cyclo-(GNSRV), cyclo-(VGAAA), adopted a relatively structured  $\beta_{II'} + \alpha_R$  configuration (58%; Table S4), suggesting that it might be possible that any cyclic pentapeptide containing the VG motif would have a rather strong preference for the  $\beta_{II'} + \alpha_R$  configuration regardless of the rest of the sequence. To test this hypothesis, on the basis of our scoring function, we designed a negative control, cyclo-(GFDNV) (highlighted in red in Figure SB), which contained the VG motif but had a low score for the  $\beta_{II'} + \alpha_R$  configuration. BE-META simulations showed that although the most populated cluster of cyclo-(GFDNV) still adopted a type II'  $\beta$  turn at residues 1GF<sup>2</sup> and an  $\alpha_R$  turn at N<sup>4</sup>, its population was, however, a mere 14.7% (Figure 6B).

To corroborate the simulation results of our negative control, we synthesized and characterized cyclo-(GFDNV) using NMR spectroscopy (Figures S7–S10, Tables S9, and S10). Overall, specific NOEs and  $J$  values consistent with a single predominant structure, as observed for cyclo-(GNSRV), were not observed for cyclo-(GFDNV). For instance, instead of a distinct, selective pattern of H<sub>N</sub>–H<sub>N</sub> NOEs, we observed four out of the five possible H<sub>N</sub>–H<sub>N</sub> NOEs (Figure 7B and Table S9). This indicates that no one single structure predominates in solution but that multiple different structures with various underlying turn combinations are present. Also,  $J$  values allowed estimation of  $\phi$  angles for Asp<sup>3</sup> and Val<sup>5</sup>. Both of these values were estimated at  $-120 \pm 30^\circ$ , which was not consistent with an  $\alpha$  turn at either residue (Table S10). Finally, we observed an additional set of peaks within the NMR spectrum of cyclo-(GFDNV) that integrated to roughly 33% of the total peak volume (Figure S11). These are consistent with the presence of two or more conformations within the ensemble that are stable on the NMR timescale. This is another clear indicator that this peptide does not have a single predominant structure in aqueous solution.

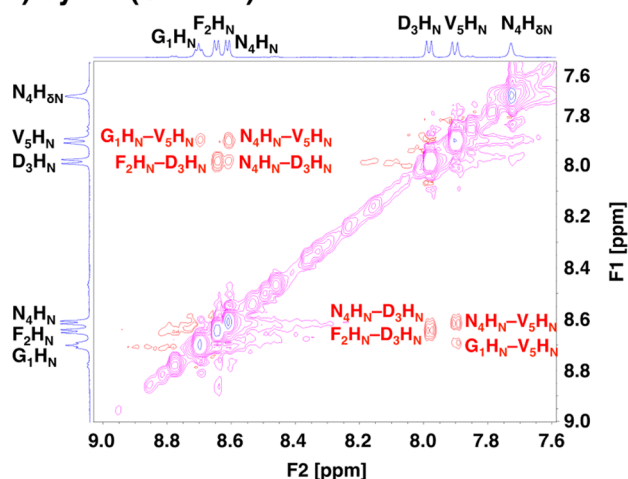
CD spectroscopy is complementary to NMR and provides a low-resolution but informative measurement of the extent of peptide structure in solution. As shown in Figure 7C, the CD



## (A) cyclo-(GNSRV)



## (B) cyclo-(GFDNV)



## (C)

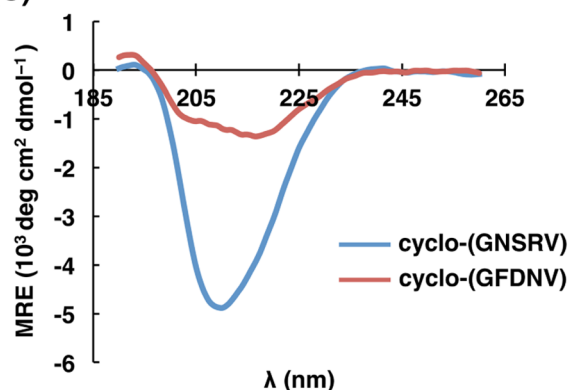


**Figure 7.** Structural characterization of cyclo-(GNSRV) and cyclo-(GFDNV). (A)  $H_N$  region of ROESY spectrum (red, magenta) for cyclo-(GNSRV). TOCSY spectrum (blue, cyan) is overlaid to highlight separate spin systems. Two ROESY cross-peaks were observed in this region, between  $N_2H_N$  and  $S_3H_N$  and between  $R_4H_N$  and  $V_5H_N$ . (B)  $H_N$  region of ROESY and TOCSY spectra for cyclo-(GFDNV). Four different ROESY  $N_H$ - $N_H$  cross-peaks were observed. (C) Circular dichroism spectra for both cyclic peptides at 87.5  $\mu$ M in aqueous solution at 20  $^{\circ}$ C, plotted as mean residue ellipticity (MRE).

spectra of cyclo-(GNSRV) and cyclo-(GFDNV) show broad minima between 208 and 218 nm, consistent with mixed  $\alpha$ -

helical and  $\beta$ -sheet structures. The negative ellipticity from cyclo-(GNSRV) is roughly fourfold more intense than that of cyclo-(GFDNV). Although it is difficult to calculate the degree of structure accurately from CD data for cyclic peptides this small, these data do indicate a much higher degree of structure for cyclo-(GNSRV) compared to cyclo-(GFDNV).

## CONCLUSIONS

In summary, using an efficient enhanced sampling method tailored for CPs, we characterized the structural ensembles of more than 70 head-to-tail cyclized pentapeptides. We demonstrated the value of these data by using them to rationally design a CP with a high degree of structure in water. We note that this designed CP sequence is well structured despite a lack of proline residues. Inclusion of proline is a common strategy to stabilize turn structures but limits the design space for CP development.<sup>80</sup>

Although the scoring function derived from cyclo-( $X_1X_2AAA$ ) enabled us to design well-structured CPs that adopt the  $\beta_{II'} + \alpha_R$  turn combination, the distribution of the scores shows that most sequences are likely not well structured (Figure 5B). Furthermore, the scores for the other turn combinations (such as  $\beta_I + \alpha_R$ ) are all minimal, suggesting that it would be extremely unlikely to favor these conformations using simple sequence substitutions. For example, cyclo-(AFDAG) has the highest score to adopt  $\beta_I + \alpha_R$  with the type I  $\beta$  turn at  $^1AF^2$  and the tight  $\alpha_R$  turn at  $A^4$ . However, this score is only 0.208. BE-META simulation of cyclo-(AFDAG) shows that indeed the top cluster of this CP was  $\beta_I + \alpha_R$  however, with a population of <30%. Therefore, to design well-structured cyclic pentapeptides that adopt conformations other than the  $\beta_{II'} + \alpha_R$  turn combination demonstrated here, non-natural amino acids are likely needed. D-Amino acids are a logical choice, although incorporating other non-natural amino acids, such as N-methylated amino acids,  $\beta$ -amino acids and proline analogs may also prove to be useful tools for CP design. The effects of incorporating these non-natural amino acids are currently being investigated. The simulation platform reported here is also not limited to cyclic pentapeptides or head-to-tail cyclized peptides and can be readily extended to larger systems or macrocycles cyclized by other linking chemistries. This work is a clear demonstration of how rigorous, explicit-solvent simulation methods are opening new opportunities to rationally design CPs with desired structures, providing a platform to rationally design novel CPs.

## ASSOCIATED CONTENT

### Supporting Information

The Supporting Information is available free of charge on the ACS Publications website at DOI: 10.1021/acs.jpcb.8b01747.

Populations of 16 turn combinations from simulations of cyclo-( $X_1X_2AAA$ );  $^1H$  1D,  $^1H$ - $^1H$  2D TOCSY, and  $^1H$ - $^1H$  2D ROESY NMR spectra of cyclo-(GNSRV) and cyclo-(GFDNV); comparison of  $^1H$  1D NMR spectra of cyclo-(GNSRV) and cyclo-(GFDNV) after 6 weeks of incubation; thermodynamics decompositions for cyclo-(GGGGG) and cyclo-(AAAAA); populations and turn combinations for the top three most populated clusters of cyclo-( $X_1AAAA$ ) and cyclo-( $X_1X_2AAA$ ); highest-scoring sequences from neighbor analysis; thermodynamic decomposition for cyclo-(GNSRV) and

five parent sequences; NOEs and *J*-coupling values for cyclo-(GNSRV) and cyclo-(GFDNV) (PDF)

## AUTHOR INFORMATION

### Corresponding Author

\*E-mail: [yu-shan.lin@tufts.edu](mailto:yu-shan.lin@tufts.edu).

### ORCID

Peng Dai: 0000-0002-4581-3473

Bradley L. Pentelute: 0000-0002-7242-801X

Joshua A. Kritzer: 0000-0003-2878-6781

Yu-Shan Lin: 0000-0001-6460-2877

### Author Contributions

<sup>§</sup>D.P.S. and S.M.M. contributed equally.

### Notes

The authors declare no competing financial interest.

## ACKNOWLEDGMENTS

We thank the support of the Tufts start-up fund, the Knez Family Faculty Investment Fund, and the National Institute of General Medical Sciences of the National Institutes of Health under award number R01GM124160 for Y.-S.L., Sontag Foundation Distinguished Scientist Award to B.L.P., and the National Science Foundation under Grant No. (1507456) for J.A.K. This work utilized NMR instrumentation that was purchased with funding from a National Institutes of Health SIG grant (S10OD020073). The content is solely the responsibility of the authors and does not necessarily represent the official views of the National Institutes of Health. We thank Dr. Kamlesh Makwana for assistance with NMR data acquisition and interpretation.

## REFERENCES

- (1) Sánchez-Quesada, J.; Kim, H. S.; Ghadiri, M. R. A Synthetic Pore-Mediated Transmembrane Transport of Glutamic Acid. *Angew. Chem., Int. Ed.* **2001**, *40*, 2503–2506.
- (2) Brea, R. J.; Castedo, L.; Granja, J. R.; Herranz, M. A.; Sanchez, L.; Martin, N.; Seitz, W.; Guldi, D. M. Electron Transfer in Me-Blocked Heterodimeric  $\alpha,\gamma$ -Peptide Nanotubular Donor–Acceptor Hybrids. *Proc. Natl. Acad. Sci. U.S.A.* **2007**, *104*, 5291–5294.
- (3) Hourani, R.; Zhang, C.; van der Weegen, R.; Ruiz, L.; Li, C.; Keten, S.; Helms, B. A.; Xu, T. Processable Cyclic Peptide Nanotubes with Tunable Interiors. *J. Am. Chem. Soc.* **2011**, *133*, 15296–15299.
- (4) Xiong, J.-P.; Stehle, T.; Zhang, R.; Joachimiak, A.; Frech, M.; Goodman, S. L.; Arnaut, M. A. Crystal Structure of the Extracellular Segment of Integrin  $\alpha_v\beta_3$  in Complex with an Arg–Gly–Asp Ligand. *Science* **2002**, *296*, 151–155.
- (5) Horswill, A. R.; Benkovic, S. J. Cyclic Peptides, A Chemical Genetics Tool for Biologists. *Cell Cycle* **2005**, *4*, 552–555.
- (6) Demmer, O.; Frank, A. O.; Hagn, F.; Schottelius, M.; Marinelli, L.; Cosconati, S.; Brack-Werner, R.; Kremb, S.; Wester, H.-J.; Kessler, H. A Conformationally Frozen Peptoid Boosts CXCR4 Affinity and Anti-HIV Activity. *Angew. Chem., Int. Ed.* **2012**, *51*, 8110–8113.
- (7) Joo, S.-H. Cyclic Peptides as Therapeutic Agents and Biochemical Tools. *Biomol. Ther.* **2012**, *20*, 19–26.
- (8) Miranda, E.; Nordgren, I. K.; Male, A. L.; Lawrence, C. E.; Hoakwie, F.; Cuda, F.; Court, W.; Fox, K. R.; Townsend, P. A.; Packham, G. K.; et al. A Cyclic Peptide Inhibitor of HIF-1 Heterodimerization That Inhibits Hypoxia Signaling in Cancer Cells. *J. Am. Chem. Soc.* **2013**, *135*, 10418–10425.
- (9) Kling, A.; Lukat, P.; Almeida, D. V.; Bauer, A.; Fontaine, E.; Sordello, S.; Zaburanyi, N.; Herrmann, J.; Wenzel, S. C.; Konig, C.; et al. Targeting DnaN for Tuberculosis Therapy using Novel Griselimycins. *Science* **2015**, *348*, 1106–1112.
- (10) Morse, R. P.; Willett, J. L. E.; Johnson, P. M.; Zheng, J.; Credali, A.; Iniguez, A.; Nowick, J. S.; Hayes, C. S.; Goulding, C. W. Diversification of  $\beta$ -Augmentation Interactions Between CDI Toxin/Immunity Proteins. *J. Mol. Biol.* **2015**, *427*, 3766–3784.
- (11) Tapeinou, A.; Matsoukas, M.-T.; Simal, C.; Tselios, T. Cyclic Peptides on a Merry-Go-Round: Towards Drug Design. *Biopolymers* **2015**, *104*, 453–461.
- (12) Cardote, T. A. F.; Ciulli, A. Cyclic and Macrocyclic Peptides as Chemical Tools To Recognise Protein Surfaces and Probe Protein–Protein Interactions. *ChemMedChem* **2016**, *11*, 787–794.
- (13) Ryan, D. P.; Matthews, J. M. Protein–Protein Interactions in Human Disease. *Curr. Opin. Struct. Biol.* **2005**, *15*, 441–446.
- (14) Gonzalez, M. W.; Kann, M. G. Chapter 4: Protein Interactions and Disease. *PLoS Comput. Biol.* **2012**, *8*, No. e1002819.
- (15) Arkin, M. R.; Tang, Y.; Wells, J. A. Small-Molecule Inhibitors of Protein–Protein Interactions: Progressing toward the Reality. *Chem. Biol.* **2014**, *21*, 1102–1114.
- (16) Milroy, L.-G.; Grossmann, T. N.; Hennig, S.; Brunsveld, L.; Ottmann, C. Modulators of Protein–Protein Interactions. *Chem. Rev.* **2014**, *114*, 4695–4748.
- (17) Kopple, K. D.; Go, A.; Logan, R. J. J.; Savrda, J. Conformations of Cyclic Peptides. VI. Factors Influencing Mono-, 1,4-Di-, and 1,2,4-Trisubstituted Cyclic Hexapeptide Backbones. *J. Am. Chem. Soc.* **1972**, *94*, 973–981.
- (18) Tonelli, A. E.; Brewster, A. I. Conformational Characteristics in Solution of the Cyclic Hexapeptide Gly–Gly–D-Ala–D-Ala–Gly–Gly. *J. Am. Chem. Soc.* **1972**, *94*, 2851–2854.
- (19) Kopple, K. D.; Go, A.; Schamper, T. J. Conformation of Cyclic Peptides. 10. Conformational Averaging in Peptides with the Sequence Cyclo-(Gly-D-Xxx-L-Yyy)<sub>2</sub>. *J. Am. Chem. Soc.* **1978**, *100*, 4289–4295.
- (20) Blout, E. R. Cyclic Peptides: Past, Present, and Future. *Biopolymers* **1981**, *20*, 1901–1912.
- (21) Varughese, K. I.; Kartha, G.; Kopple, K. D. Crystal Structure and Conformation of Cyclo-(Glycyl–D-Leucyl–L-Leucyl)<sub>2</sub>. *J. Am. Chem. Soc.* **1981**, *103*, 3310–3313.
- (22) Yang, C.-H.; Brown, J. N.; Kopple, K. D. Crystal Structure and Solution Studies of the Molecular Conformation of the Cyclic Hexapeptide Cyclo-(Gly–L-His–Gly–L-Ala–L-Tyr–Gly). *J. Am. Chem. Soc.* **1981**, *103*, 1715–1719.
- (23) Kopple, K. D.; Wang, Y. S.; Cheng, A. G.; Bhandary, K. K. Conformations of Cyclic Octapeptides. 5. Crystal Structure of Cyclo(Cys–Gly–Pro–Phe)<sub>2</sub> and Rotating Frame Relaxation (*T*<sub>1ρ</sub>) NMR Studies of Internal Mobility in Cyclic Octapeptides. *J. Am. Chem. Soc.* **1988**, *110*, 4168–4176.
- (24) Stradley, S. J.; Rizo, J.; Bruch, M. D.; Stroup, A. N.; Gierasch, L. M. Cyclic Pentapeptides as Models for Reverse Turns: Determination of the Equilibrium Distribution Between Type I and Type II Conformations of Pro–Asn and Pro–Ala  $\beta$ -turns. *Biopolymers* **1990**, *29*, 263–287.
- (25) Alberg, D. G.; Schreiber, S. L. Structure-Based Design of a Cyclophilin–Calcineurin Bridging Ligand. *Science* **1993**, *262*, 248–250.
- (26) Kopple, K. D.; Bean, J. W.; Bhandary, K. K.; Briand, J.; D'Ambrosio, C. A.; Peishoff, C. E. Conformational Mobility in Cyclic Oligopeptides. *Biopolymers* **1993**, *33*, 1093–1099.
- (27) Marshall, G. R.; Beusen, D. D.; Nikiforovich, G. V. In *Peptides: Synthesis, Structures, and Applications*; Gutte, B., Ed.; Academic Press, Inc.: San Diego, CA, 1995; Vol. 27, pp 193–245.
- (28) Beck, J. G.; Chatterjee, J.; Laufer, B.; Kiran, M. U.; Frank, A. O.; Neubauer, S.; Ovadia, O.; Greenberg, S.; Gilon, C.; Hoffman, A.; et al. Intestinal Permeability of Cyclic Peptides: Common Key Backbone Motifs Identified. *J. Am. Chem. Soc.* **2012**, *134*, 12125–12133.
- (29) Bhowmick, A.; Brookes, D. H.; Yost, S. R.; Dyson, H. J.; Forman-Kay, J. D.; Gunter, D.; Head-Gordon, M.; Hura, G. L.; Pande, V. S.; Wemmer, D. E.; et al. Finding Our Way in the Dark Proteome. *J. Am. Chem. Soc.* **2016**, *138*, 9730–9742.
- (30) Brookes, D. H.; Head-Gordon, T. Experimental Inferential Structure Determination of Ensembles for Intrinsically Disordered Proteins. *J. Am. Chem. Soc.* **2016**, *138*, 4530–4538.

- (31) Best, R. B. Computational and Theoretical Advances in Studies of Intrinsically Disordered Proteins. *Curr. Opin. Struct. Biol.* **2017**, *42*, 147–154.
- (32) Bonomi, M.; Heller, G. T.; Camilloni, C.; Vendruscolo, M. Principles of Protein Structural Ensemble Determination. *Curr. Opin. Struct. Biol.* **2017**, *42*, 106–116.
- (33) Riemann, R. N.; Zacharias, M. Reversible Scaling of Dihedral Angle Barriers During Molecular Dynamics to Improve Structure Prediction of Cyclic Peptides. *J. Pept. Res.* **2004**, *63*, 354–364.
- (34) Spitaleri, A.; Ghitti, M.; Mari, S.; Alberici, L.; Traversari, C.; Rizzardi, G.-P.; Musco, G. Use of Metadynamics in the Design of isoDGR-Based  $\alpha\beta_3$  Antagonists To Fine-Tune the Conformational Ensemble. *Angew. Chem., Int. Ed.* **2011**, *50*, 1832–1836.
- (35) Voelz, V. A.; Dill, K. A.; Chorny, I. Peptoid Conformational Free Energy Landscapes From Implicit-Solvent Molecular Simulations in AMBER. *Biopolymers* **2011**, *96*, 639–650.
- (36) Butterfoss, G. L.; Yoo, B.; Jaworski, J. N.; Chorny, I.; Dill, K. A.; Zuckermann, R. N.; Bonneau, R.; Kirshenbaum, K.; Voelz, V. A. *De Novo* Structure Prediction and Experimental Characterization of Folded Peptoid Oligomers. *Proc. Natl. Acad. Sci. U.S.A.* **2012**, *109*, 14320–14325.
- (37) Chen, Y.; Deng, K.; Qiu, X.; Wang, C. Visualizing Cyclic Peptide Hydration at the Single-Molecule Level. *Sci. Rep.* **2013**, *3*, No. 2461.
- (38) Damas, J. M.; Filipe, L. C. S.; Campos, S. R. R.; Lousa, D.; Victor, B. L.; Baptista, A. M.; Soares, C. M. Predicting the Thermodynamics and Kinetics of Helix Formation in a Cyclic Peptide Model. *J. Chem. Theory Comput.* **2013**, *9*, 5148–5157.
- (39) Oakley, M. T.; Johnston, R. L. Exploring the Energy Landscapes of Cyclic Tetrapeptides with Discrete Path Sampling. *J. Chem. Theory Comput.* **2013**, *9*, 650–657.
- (40) Oakley, M. T.; Oheix, E.; Peacock, A. F. A.; Johnston, R. L. Computational and Experimental Investigations into the Conformations of Cyclic Tetra- $\alpha/\beta$ -Peptides. *J. Phys. Chem. B* **2013**, *117*, 8122–8134.
- (41) Merten, C.; Li, F.; Bravo-Rodriguez, K.; Sanchez-Garcia, E.; Xu, Y.; Sander, W. Solvent-Induced Conformational Changes in Cyclic Peptides: A Vibrational Circular Dichroism Study. *Phys. Chem. Chem. Phys.* **2014**, *16*, 5627–5633.
- (42) Quartararo, J. S.; Eshelman, M. R.; Peraro, L.; Yu, H.; Baleja, J. D.; Lin, Y.-S.; Kritzer, J. A. A Bicyclic Peptide Scaffold Promotes Phosphotyrosine Mimicry and Cellular Uptake. *Bioorg. Med. Chem.* **2014**, *22*, 6387–6391.
- (43) Razavi, A. M.; Wuest, W. M.; Voelz, V. A. Computational Screening and Selection of Cyclic Peptide Hairpin Mimetics by Molecular Simulation and Kinetic Network Models. *J. Chem. Inf. Model.* **2014**, *54*, 1425–1432.
- (44) Paissoni, C.; Ghitti, M.; Belvisi, L.; Spitaleri, A.; Musco, G. Metadynamics Simulations Rationalise the Conformational Effects Induced by N-Methylation of RGD Cyclic Hexapeptides. *Chem. – Eur. J.* **2015**, *21*, 14165–14170.
- (45) Wakefield, A. E.; Wuest, W. M.; Voelz, V. A. Molecular Simulation of Conformational Pre-Organization in Cyclic RGD Peptides. *J. Chem. Inf. Model.* **2015**, *55*, 806–813.
- (46) Yedvabny, E.; Nerenberg, P. S.; So, C.; Head-Gordon, T. Disordered Structural Ensembles of Vasopressin and Oxytocin and Their Mutants. *J. Phys. Chem. B* **2015**, *119*, 896–905.
- (47) Yu, H.; Lin, Y.-S. Toward Structure Prediction of Cyclic Peptides. *Phys. Chem. Chem. Phys.* **2015**, *17*, 4210–4219.
- (48) Geng, H.; Jiang, F.; Wu, Y.-D. Accurate Structure Prediction and Conformational Analysis of Cyclic Peptides with Residue-Specific Force Fields. *J. Phys. Chem. Lett.* **2016**, *7*, 1805–1810.
- (49) McHugh, S. M.; Rogers, J. R.; Yu, H.; Lin, Y.-S. Insights Into How Cyclic Peptides Switch Conformations. *J. Chem. Theory Comput.* **2016**, *12*, 2480–2488.
- (50) McHugh, S. M.; Yu, H.; Slough, D. P.; Lin, Y.-S. Mapping the Sequence–Structure Relationships of Simple Cyclic Hexapeptides. *Phys. Chem. Chem. Phys.* **2017**, *19*, 3315–3324.
- (51) Slough, D. P.; Yu, H.; McHugh, S. M.; Lin, Y.-S. Towards Accurately Modeling N-Methylated Cyclic Peptides. *Phys. Chem. Chem. Phys.* **2017**, *19*, 5377–5388.
- (52) Pettersen, E. F.; Goddard, T. D.; Huang, C. C.; Couch, G. S.; Greenblatt, D. M.; Meng, E. C.; Ferrin, T. E. UCSF Chimera—A Visualization System for Exploratory Research and Analysis. *J. Comput. Chem.* **2004**, *25*, 1605–1612.
- (53) Bussi, G.; Donadio, D.; Parrinello, M. Canonical Sampling Through Velocity Rescaling. *J. Chem. Phys.* **2007**, *126*, No. 014101.
- (54) Cheng, A.; Merz, K. M., Jr. Application of the Nosé–Hoover Chain Algorithm to the Study of Protein Dynamics. *J. Phys. Chem.* **1996**, *100*, 1927–1937.
- (55) Lingenheil, M.; Denschlag, R.; Reichold, R.; Tavan, P. The “Hot-Solvent/Cold-Solute” Problem Revisited. *J. Chem. Theory Comput.* **2008**, *4*, 1293–1306.
- (56) Berendsen, H. J. C.; Postma, J. P. M.; van Gunsteren, W. F.; DiNola, A.; Haak, J. R. Molecular Dynamics with Coupling to an External Bath. *J. Chem. Phys.* **1984**, *81*, 3684–3690.
- (57) Hess, B.; Bekker, H.; Berendsen, H. J. C.; Fraaije, J. G. E. M. LINCS: A Linear Constraint Solver for Molecular Simulations. *J. Comput. Chem.* **1997**, *18*, 1463–1472.
- (58) Hockney, R. W. The Potential Calculation and Some Applications. *Methods Comput. Phys.* **1970**, *9*, 135–211.
- (59) Essmann, U.; Perera, L.; Berkowitz, M. L.; Darden, T.; Lee, H.; Pedersen, L. G. A Smooth Particle Mesh Ewald Method. *J. Chem. Phys.* **1995**, *103*, 8577–8593.
- (60) Allen, M. P.; Tildesley, D. J., Eds. *Computer Simulations of Liquids*; Oxford University Press: New York, 1987.
- (61) Zhou, C.-Y.; Jiang, F.; Wu, Y.-D. Residue-Specific Force Field Based on Protein Coil Library. RSFF2: Modification of AMBER ff99SB. *J. Phys. Chem. B* **2015**, *119*, 1035–1047.
- (62) Jorgensen, W. L.; Chandrasekhar, J.; Madura, J. D.; Impey, R. W.; Klein, M. L. Comparison of Simple Potential Functions for Simulating Liquid Water. *J. Chem. Phys.* **1983**, *79*, 926–935.
- (63) Hess, B.; Kutzner, C.; van der Spoel, D.; Lindahl, E. GROMACS 4: Algorithms for Highly Efficient, Load-Balanced, and Scalable Molecular Simulation. *J. Chem. Theory Comput.* **2008**, *4*, 435–447.
- (64) Tribello, G. A.; Bonomi, M.; Branduardi, D.; Camilloni, C.; Bussi, G. PLUMED 2: New Feathers for an Old Bird. *Comput. Phys. Commun.* **2014**, *185*, 604–613.
- (65) Mu, Y.; Nguyen, P. H.; Stock, G. Energy Landscape of a Small Peptide Revealed by Dihedral Angle Principal Component Analysis. *Proteins: Struct., Funct., Bioinf.* **2005**, *58*, 45–52.
- (66) Sittel, F.; Jain, A.; Stock, G. Principal Component Analysis of Molecular Dynamics: On the Use of Cartesian vs. Internal Coordinates. *J. Chem. Phys.* **2014**, *141*, No. 014111.
- (67) Rodriguez, A.; Laio, A. Clustering by Fast Search and Find of Density Peaks. *Science* **2014**, *344*, 1492–1496.
- (68) King, B. M.; Tidor, B. MIST: Maximum Information Spanning Trees for Dimension Reduction of Biological Data Sets. *Bioinformatics* **2009**, *25*, 1165–1172.
- (69) King, B. M.; Silver, N. W.; Tidor, B. Efficient Calculation of Molecular Configurational Entropies Using an Information Theoretic Approximation. *J. Phys. Chem. B* **2012**, *116*, 2891–2904.
- (70) Fleck, M.; Polyansky, A. A.; Zagrovic, B. PARENT: A Parallel Software Suite for the Calculation of Configurational Entropy in Biomolecular Systems. *J. Chem. Theory Comput.* **2016**, *12*, 2055–2065.
- (71) Mijalis, A. J.; Thomas, D. A., III; Simon, M. D.; Adamo, A.; Beaumont, R.; Jensen, K. F.; Pentelute, B. L. A Fully Automated Flow-Based Approach for Accelerated Peptide Synthesis. *Nat. Chem. Biol.* **2017**, *13*, 464–466.
- (72) Karle, I. L. Crystal Structure and Conformation of Cyclo-(GlycylProlylGlycyl-D-AlanylProlyl) Containing 4→1 and 3→1 Intramolecular Hydrogen Bonds. *J. Am. Chem. Soc.* **1978**, *100*, 1286–1289.
- (73) Gurrath, M.; Muller, G.; Kessler, H.; Aumailley, M.; Timpl, R. Conformation/Activity Studies of Rationally Designed Potent Anti-Adhesive RGD Peptides. *Eur. J. Biochem.* **1992**, *210*, 911–921.



(74) Mierke, D. F.; Kurz, M.; Kessler, H. Peptide Flexibility and Calculations of an Ensemble of Molecules. *J. Am. Chem. Soc.* **1994**, *116*, 1042–1049.

(75) Nagarajaram, H. A.; Ramakrishnan, C. Stereochemical Studies on Cyclic Peptides: Detailed Energy Minimization Studies on Hydrogen Bonded All-*Trans* Cyclic Pentapeptide Backbones. *J. Biosci.* **1995**, *20*, 591–611.

(76) Davies, J. S. In *Cyclic Polymers*; Semlyen, E. R., Ed.; Kluwer Academic Publishers: Netherlands, 2000; pp 85–124.

(77) Nikiforovich, G. V.; Kövér, K. E.; Zhang, W.-J.; Marshall, G. R. Cyclopentapeptides as Flexible Conformational Templates. *J. Am. Chem. Soc.* **2000**, *122*, 3262–3273.

(78) Zhang, X.; Nikiforovich, G. V.; Marshall, G. R. Conformational Templates for Rational Drug Design: Flexibility of Cyclo(D-Pro<sub>1</sub>–Ala<sub>2</sub>–Ala<sub>3</sub>–Ala<sub>4</sub>–Ala<sub>5</sub>) in DMSO Solution. *J. Med. Chem.* **2007**, *50*, 2921–2925.

(79) Demmer, O.; Frank, A. O.; Kessler, H. In *Peptide and Protein Design for Biopharmaceutical Applications*; Jensen, K. J., Ed.; John Wiley & Sons, Ltd.: Chichester, U.K., 2009; pp 133–176.

(80) Hosseinzadeh, P.; Bhardwaj, G.; Mulligan, V. K.; Shortridge, M. D.; Craven, T. W.; Pardo-Avila, F.; Rettie, S. A.; Kim, D. E.; Silva, D.-A.; Ibrahim, Y. M.; et al. Comprehensive Computational Design of Ordered Peptide Macrocycles. *Science* **2017**, *358*, 1461–1466.

#### ■ NOTE ADDED AFTER ASAP PUBLICATION

Due to a production error, this paper published ASAP on March 28, 2018 with a duplication of text. The corrected version was reposted on March 29, 2018.